Assessment of methane levels throughout a temperate reservoir area using remote sensing data

Oleg Nikitin[1,*], *Nadezhda* Stepanova[2], *Svetlana* Gubeeva[2], *Ruslan* Kuzmin[1], and *Venera* Latypova[2]

[1]Ekoaudit LLC, 420061, Kazan, Russia
[2]Kazan Federal University, 420097, Kazan, Russia

Abstract. Aquatic ecosystems are significant methane (CH_4) emitters, potentially surpassing direct anthropogenic sources. Despite the advantages of satellite monitoring, its application for assessing methane content over freshwater bodies is not commonly encountered in scientific publications. Therefore, this study aims to assess methane levels in the atmosphere in and around the temperate reservoir area (Kuibyshev Reservoir, Russia) using Sentinel-5P/TROPOMI remote sensing data. The spatial distribution of CH_4 content across the study area was heterogeneous and exhibited a latitudinal dependence, with concentrations decreasing from south to north. Seasonal variability in methane levels is observed, with the lowest values in spring and the highest in autumn. The average CH_4 concentration over the period 2019–2023 was 1860±13 ppb. Additionally, a consistent trend of increasing annual methane background levels has been observed (up to 1878±11 ppb in 2023). Differences in methane levels are noted across different land cover types, with higher values typically observed above anthropogenically transformed landscapes, while minimal ones are found over extensive forested areas and the waters of the Kuibyshev Reservoir.

1 Introduction

In the contemporary world, the urgency of addressing climate change is increasingly evident, necessitating the attention of specialists across various scientific domains. 2023 was the warmest year on record at 1.45±0.12 °C above the pre-industrial average. Concentrations of the three main greenhouse gases (GHGs) – carbon dioxide (CO_2), methane (CH_4), and nitrous oxide (N_2O) – reached record high-observed levels [1]. Methane emissions into the atmosphere stand out as a significant factor of concern in this regard. As one of the most potent greenhouse gases, its direct radiative impact positions it as the second most influential human-induced driver of climate change throughout historical period. CH_4 accounts for approximately 30% of the global temperature rise since the onset of the Industrial Revolution. While CO_2 exerts a more prolonged effect, methane drives short-term warming dynamics, contributing to at least 25% of current anthropogenic

* Corresponding author: olnova@mail.ru

global warming. It is crucial to highlight that methane concentrations in the atmosphere have more than doubled over the past two centuries, primarily attributable to human activities. This escalation underscores the significant role of anthropogenic factors in the CH_4 budget, emphasizing the urgent need for targeted mitigation strategies across various sectors to address this alarming trend [2, 3].

Aquatic ecosystems, including wetlands, freshwater lakes, reservoirs, streams and rivers, estuarine systems, coastal areas, and marine systems, play a significant role as methane emitters [4]. A recent review on this topic suggests that their emissions are potentially a larger source of CH_4 than direct anthropogenic sources, such as agriculture or fossil fuel combustion. And overall, aquatic ecosystems and wetlands account for at least half of the total methane emissions budget [5].

Reservoirs, artificial water bodies formed by the construction of dams, are widespread globally [6]. These dam-reservoir systems serve various purposes, including hydroelectric power generation, flood control, water supply, recreation, and navigation. Reservoirs are sites of intense carbon processing in the landscape. Carbon input into lentic ecosystems, whether from watershed runoff or internal primary production, undergoes microbial transformations, often resulting in the production of greenhouse gases, including methane [7-12]. These emissions occur through various pathways such as diffusion (direct from sediments and/or the water surface), ebullition (bubbling), degassing from turbines and spillways, advection through plants, exposure of anoxic CH_4-rich deep waters to the atmosphere during convective mixing (turnover), and water drawdown events [13-15].

Scientific approaches for assessing methane formation processes in a reservoir and their intensity include instrumental methods for measuring CH_4 emissions, sediment characteristics analysis, and predictive modeling based on factors like sediment age and nitrogen content [16, 17]. Instrumental assessment (e.g., active sensors, eddy covariance, boundary layer methods, floating chambers, and bubble traps) provides direct data on methane formation intensity. This involves techniques for quantifying CH_4 fluxes from bottom sediments, water-atmosphere interfaces, and ebullition processes [15, 18-20]. Studying sediment characteristics, such as total carbon content, nitrogen concentration, and organic matter flux, helps understand the factors influencing methane formation rates in bottom sediments. Analyzing sediment properties provides insights into the potential for methane production [21]. Predictive models based on factors such as sediment age, carbon and nitrogen content offer a systematic approach to estimating methane formation rates in reservoirs. These models help understand the relationship between key variables and CH_4 production intensity across different biogeographic regions [10, 17, 22]. By combining these approaches, researchers can gain a comprehensive understanding of methane formation processes in reservoirs, assess the intensity of CH_4 emissions, and predict methane production rates based on sediment characteristics and environmental factors.

Satellite-based techniques utilize remote sensing technology to detect and quantify CH_4 concentrations in the atmosphere. These methods involve observing CH_4 column abundance from satellite platforms (such as SCIAMACHY, GOSAT, TROPOMI, GHGSat, and others), significantly increasing spatial and temporal coverage for monitoring methane emissions [23-27]. Ground-based techniques offer advantages in terms of accuracy and reliability compared to satellite-based methods because they provide direct and precise measurements of methane emissions from localized sources, ensuring high confidence in emission estimation within the sampled area. These techniques are independent of atmospheric modeling methods and can offer detailed insights into emission sources and rates. However, ground-based methods are limited in their coverage and may not capture emissions from a broader area or multiple sources simultaneously.

Nonetheless despite the advantages of satellite monitoring, its application for assessing methane content over aquatic ecosystems is not commonly encountered in scientific

publications. Therefore, the aim of this study is to attempt to assess the methane levels in the atmosphere in and around the Kuibyshev Reservoir area based on remote sensing data.

2 Materials and methods

2.1 Study area

The Kuibyshev Reservoir is situated in the Middle Volga and Lower Kama region. It was created in 1955–1957 by the construction of the Zhiguli Hydroelectric Station Dam on the Volga River near Zhigulyovsk and Tolyatti in the Samara Oblast. The Kuibyshev Reservoir is the largest reservoir in the Volga-Kama Cascade and one of the largest reservoirs in the world. It stretches for a total length of 510 km along the flooded channel of the Volga River, with a maximum width of 27 km and an average depth of 9 m. The reservoir covers a surface area of 5,900 km^2 and has a total capacity of 58 km^3; approximately 16% of the reservoir is shallow (less than 3 m depth). The water body is located within five regions in Russia: the Republic of Tatarstan (50.7%), the Ulyanovsk (30.9%) and Samara (14.7%) oblasts, and the Chuvashia and Mari El republics (3.7%). In addition to the reservoir itself, the study also considered the regions of Russia where it is located (see Figure 1). The Kuibyshev Reservoir serves multiple purposes, including drinking and industrial water supply, energy generation, mining, fire safety, transportation, agriculture, fishing, forestry, and recreation. As a result, the reservoir has a sufficiently high level of pollution from nitrogen and phosphorus compounds, petroleum hydrocarbons, metals, etc. [28-30].

2.2 Satellite data processing and land cover characteristics

The study relies on methane measurements in the atmosphere using the TROPOMI data (ESA Copernicus Sentinel-5P mission). The TROPOMI is a nadir-viewing imaging spectrometer, covering wavelength ranges from ultraviolet to shortwave infrared [31]. Access to satellite data and primary operations were conducted using the Google Earth Engine (GEE) cloud platform [32]. Satellite data (OFFL L3 Product) for the five years (2019–2023) were employed in the study. The ESA WorldCover 10m v200 dataset was used to characterize the land cover of the studied area. This dataset, provided by the European Space Agency (ESA), offers a global land cover map for 2021 at a resolution of 10 meters, utilizing data from Sentinel-1 and Sentinel-2 satellites [33].

2.4 Data handling and analysis

For cartographic visualization of the data, QGIS 3.28 software was used. Map coordinates are represented as geodetic ones (WGS-84, degrees and minutes north latitude and east longitude). Administrative divisions shapefiles were accessed through the open license resource geoBoundaries Global Administrative Database [34]. Statistical analysis was performed using Statistica 10. The data were expressed as mean ± standard deviation.

3 Results and discussion

The spatial distribution of methane content across the examined area, as well as land cover classes, are depicted in Figure 1. The average methane concentration in 2023 for the surveyed territory was 1878±11 ppb. The highest average concentration was observed for Samara Oblast – 1883±8 ppb, while the lowest was for the Mari El Republic – 1866±9 ppb. The methane content in the atmosphere of the studied regions shows a latitudinal

dependency – as one moves from south to north, the concentration decreases (r = –0.52). The relationship with longitude is less pronounced (r = 0.16).

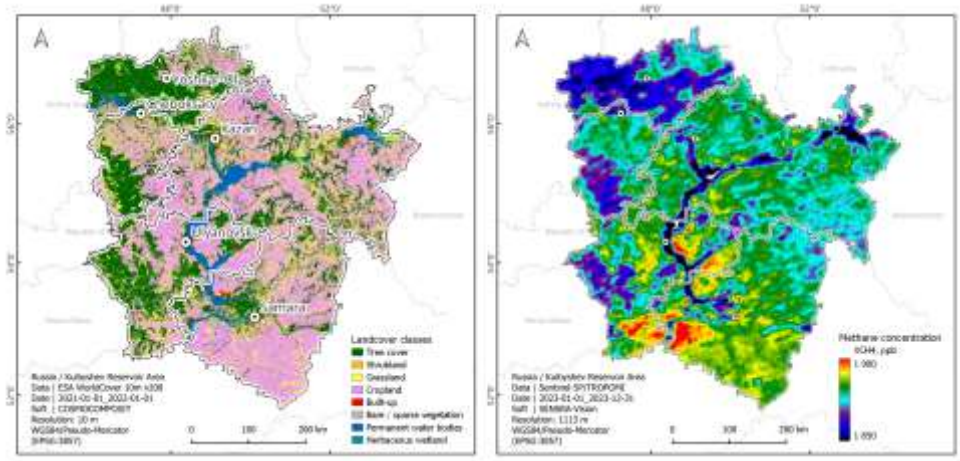

Fig. 1. Studied area. Land cover classes (left) and column-averaged dry air mixing ratio of methane (XCH_4) as parts-per-billion in 2023 (right).

The average CH_4 concentration over the period 2019–2023 was 1860±13 ppb. A consistent trend of increasing annual methane background levels has been observed. In comparison to 2019, the concentration in 2023 increased by 2.6% across the territory, which aligns with the trend previously identified in Tatarstan [35]. Additionally, significant monthly variations in methane background concentrations are evident, with peak values occurring in the fall and the lowest in the spring season (Figure 2).

The highest concentrations consistently occur near major industrial facilities and thermal power plants, while minimal levels are found in extensive forested areas and the waters of the Kuibyshev Reservoir. Elevated methane levels are also typical in populated areas, including both large urban centers and small rural settlements. Seasonal variations in CH_4 concentration are noticeable above agricultural landscapes. Cluster of artificial landscape types (Figure 3), 'Built-up' and 'Cropland', significantly differs from the other groups in terms of methane content, except for the 'Cropland-Grassland' pair, where no differences were found. The 'Grassland-Herbaceous wetland' pair also shows no significant differences in methane levels, occupying an intermediate position among the considered landscape types. Similarly, the 'Tree cover' and 'Permanent water bodies' pair exhibit similar CH_4 concentration levels.

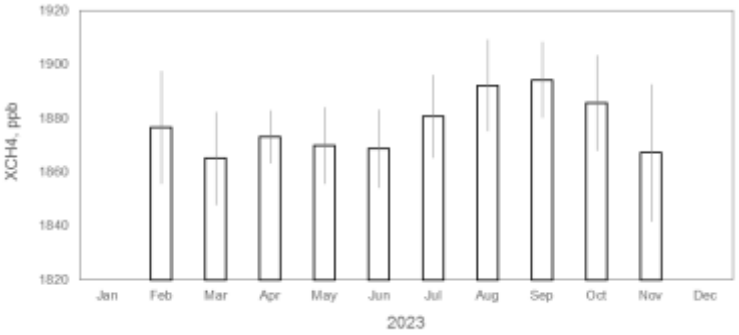

Fig. 2. Average monthly methane concentration (XCH_4) within the five examined regions in 2023.

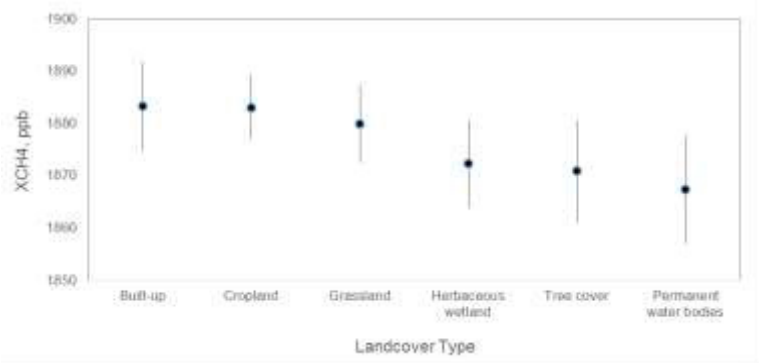

Fig. 3. Annual average methane concentration (XCH_4) above designated landscape classes in the studied area in 2023.

The methane levels directly above the Kuibyshev Reservoir's water surface from April to October 2023 (ice-free period) is shown in Figure 4. The concentration over the reservoir varied between 1735 and 1903 ppb. The highest concentrations were associated with shallow areas, while the lowest values were observed over the pelagic zones of lake-like extensions. The concentrations recorded for the water surface within the Republic of Tatarstan averaged 1847±3 ppb, closely resembling the overall mean values across the whole reservoir (1855±17 ppb). The average concentration over the reservoir during the ice-free period differed from the mean CH_4 concentration across the study area by 24 ppb.

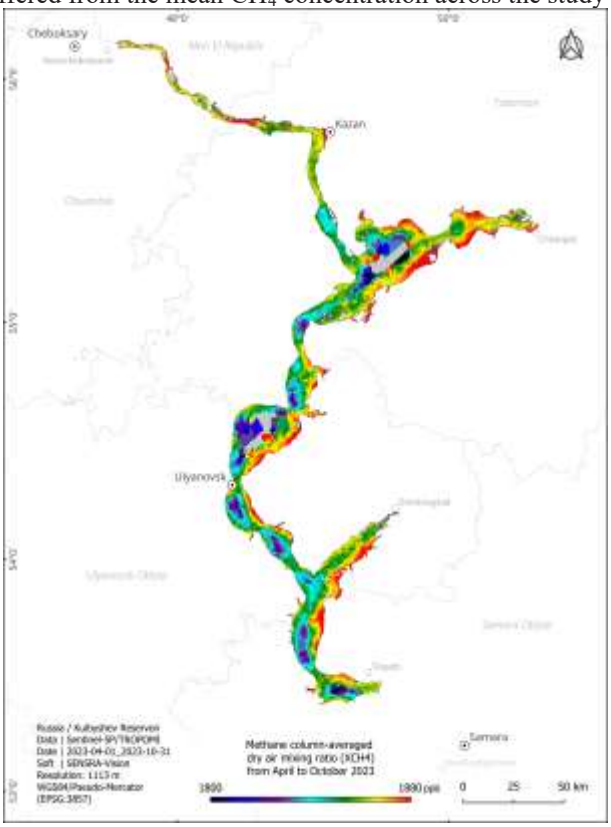

Fig. 4. Average methane concentration (April to October 2023) in the atmosphere above the Kuibyshev Reservoir waters according to Sentinel-5P/TROPOMI data.

Methane formation and emission processes are influenced by a multitude of physicochemical properties specific to each reservoir [13-15, 36, 37]. Specifically it was found [38] that the best predictors of methane emission differed by waterbody type (lakes or reservoirs), and that morphometric variables (surface area and maximum depth) were more important in lakes whereas indicators of autochthonous production (chlorophyll-*a*) were of greater importance in reservoirs. Productivity was also found to be a significant predictor of methane ebullition, whereas ecosystem morphometry and waterbody type were more important parameters for CH_4 diffusive flux prognosis.

Eutrophication of reservoirs, caused by high nutrient loadings such as total nitrogen, organic carbon, and total phosphorus, due to agricultural, industrial, and urban activities in the catchment, is also a significant contributing factor to GHGs emission [39, 40]. These factors are also typical for the Kuibyshev Reservoir [28, 41, 42]. As eutrophication progresses, the enhanced nutrients availability fuels the proliferation of algae and other aquatic plants. Subsequently these organisms decompose in an oxygen-deprived environment created by eutrophication-induced oxygen depletion. Under anaerobic conditions, organic matter undergoes decomposition by anaerobic bacteria, leading to the production and release of methane [43, 44]. However, it is worth noting that methane can also form under aerobic conditions, a phenomenon known as the 'methane paradox' (CH_4 supersaturation in oxygenated waters) [45-47]. In this case, the mechanisms involved in the production of aerobic methane by phytoplankton include photosynthesis-driven metabolism, demethylation of methyl donors driven by reactive oxygen species (ROS), methanogenesis catalyzed by nitrogenase, and demethylation of phosphonates catalyzed by C-P lyase [48].

4 Conclusion

In conclusion, it can be noted that accumulating data on the atmospheric concentrations of climate-active gases, identifying relationships between the functioning of aquatic communities in terms of carbon cycling, and understanding the impact of these communities on atmospheric GHGs concentrations are pressing tasks. Conducting such studies through ground-based measurements and remote sensing techniques (bottom-up and top-down approaches) will enable the acquisition of up-to-date data on greenhouse gas emissions and fluxes from reservoir surfaces. This will delineate their contribution to the overall GHGs flux both within the reservoir and within the catchment as a whole.

The work partially was funded by the subsidy allocated to Kazan Federal University for the state assignment in the sphere of scientific activities (No. FZSM-2024-0004).

References

1. State of the Global Climate 2023. WMO-No. 1347 (2024) https://library.wmo.int/idurl/4/68835
2. C.J. Sapart, G. Monteil, M. Prokopiou, R.S. van de Wal, J.O. Kaplan, P. Sperlich, K.M. Krumhardt, C. van der Veen, S. Houweling, M.C. Krol, T. Blunier, T. Sowers, P. Martinerie, E. Witrant, D. Dahl-Jensen, T. Röckmann, Nature, **490**, 85–88 (2012)
3. M. Saunois, A.R. Stavert, B. Poulter, P. Bousquet, J.G. Canadell et al., Earth Syst. Sci. Data, **12**, 1561–1623 (2020)
4. L.J. Hamdan, K.P. Wickland, Limnol. Oceanogr, **61**, S3–S12 (2016)

5. J.A. Rosentreter, A.V. Borges, B.R. Deemer, M.A. Holgerson, S. Liu, C. Song, J. Melack, P.A. Raymond, C.M. Duarte, G.H. Allen, D. Olefeldt, B. Poulter, T.I. Battin, B.D. Eyre, Nat. Geosci., **14**, 225–230 (2021)
6. B. Lehner, C.R. Liermann, C. Revenga, C. Vörösmarty, B. Fekete, P. Crouzet, P. Döll, M. Endejan, K. Frenken, J. Magome, C. Nilsson, J.C. Robertson, R. Rödel, N. Sindorf, D. Wisser, Front. Ecol. Environ., **9**, 494–502 (2011)
7. V.L. St. Louis, C.A. Kelly, É. Duchemin, J.W.M. Rudd, D.M. Rosenberg, BioScience, **50**, 766–775 (2000)
8. N. Barros, J. Cole, L. Tranvik, Y.T. Prairie, D. Bastviken, V.L.M. Huszar, P. del Giorgio, F. Roland, Nature Geosci., **4**, 593–596 (2011)
9. B.R. Deemer, J.A. Harrison, S. Li, J.J. Beaulieu, T. DelSontro, N. Barros, J.F. Bezerra-Neto, S.M. Powers, M.A. dos Santos, J.A. Vonk, BioScience, **66**, 949–964 (2016)
10. J.J. Beaulieu, S. Waldo, D.A. Balz, W. Barnett, A. Hall, M.C. Platz, K.M. White, J. Geophys. Res. Biogeosci. **125**, e2019JG005474 (2020)
11. J.A. Harrison, Y.T. Prairie, S. Mercier-Blais, C. Soued, Global Biogeochem. Cycles, **35**, e2020GB006888 (2021)
12. A. Martínez-García, I. Peralta-Maraver, E. Rodríguez-Velasco, G.L. Batanero, M. García-Alguacil, F. Picazo, J. Calvo, R. Morales-Baquero, F.J. Rueda, I. Reche, Limnol. Oceanogr. Lett. (2024)
13. T. DelSontro, D.F. McGinnis, S. Sobek, I. Ostrovsky, B. Wehrli, Environ. Sci. Technol., **44**, 2419–2425 (2010)
14. Y.T. Prairie, S. Mercier-Blais, J.A. Harrison, C. Soued, P. del Giorgio, A. Harby, J. Alm, V. Chanudet, R. Nahas, Environ. Model. Softw., **143**, 105117 (2021)
15. M.S. Johnson, E. Matthews, D. Bastviken, B. Deemer, J. Du, V. Genovese, J. Geophys. Res. Biogeosci., **126**, e2021JG006305 (2021)
16. A. Isidorova, C. Grasset, R. Mendonça, S. Sobek, Sci. Rep., **9**, 11017 (2019)
17. S. Moras, U.R. Zellmer, E. Hiltunen, C. Grasset, S. Sobek, J. Geophys. Res. Biogeosci., **129**, e2023JG007463 (2024)
18. V.A. Lomov, IOP Conf. Ser.: Earth Environ. Sci., **834**, 012032 (2021)
19. S. Waldo, J.J. Beaulieu, W. Barnett, D.A. Balz, M.J. Vanni, T. Williamson, J.T. Walker, Biogeosci., **18**, 5291–5311 (2021)
20. A.G. Hounshell, B.M. D'Acunha, A. Breef-Pilz, M.S. Johnson, R.Q. Thomas, C.C. Carey, J. Geophys. Res. Biogeosci., **128**, e2022JG007091 (2023)
21. M.E. Berberich, J.J. Beaulieu, T.L. Hamilton, S. Waldo, I. Buffam, Limnol. Oceanogr., **65**, 1336–1358 (2019)
22. R. Gruca-Rokosz, M. Cieśla, Sci. Total Environ., **799**, 149219 (2021)
23. S. Pandey, S. Houweling, A. Lorente, T. Borsdorff, M. Tsivlidou, A.A. Bloom, B. Poulter, Zhang Z., I. Aben, Biogeosci., **18**, 557–572 (2021)
24. B.M. Erland, A.K. Thorpe, J.A. Gamon, Environ. Sci. Technol., **56**, 23, 16567–16581 (2022)
25. S. Zhang, J. Ma, X. Zhang, C. Guo, Sci. Total Environ., **893**, 164701 (2023)
26. C. Karoff, A.L. Vara-Vela, Front. Earth Sci., **11**, 1119977 (2023)
27. K. Li, K. Bai, P. Jiao, H. Chen, H. He, L. Shao, Y. Sun, Z. Zheng, R. Li, N.-B. Chang, Remote Sens. Environ., **304** (2024)

28. O.V. Nikitin, N.Yu. Stepanova, V.Z. Latypova, Water Sci. Technol.: Water Supply, **15**, 693–700 (2015)
29. A.V. Rakhuba, Uchenye Zapiski Kazanskogo Universiteta. Seriya Estestvennye Nauki, **162**, 430–444 (2020)
30. K.V. Bespalova, A.V. Selezneva, V.A. Seleznev, IOP Conf. Ser.: Earth Environ. Sci., **607**, 012017 (2020)
31. J.P. Veefkind, I. Aben, K. McMullan, H. Förster, J. de Vries, G. Otter, J. Claas, H. J. Eskes, J. F. de Haan, Q. Kleipool, M. van Weele, O. Hasekamp, R. Hoogeveen, J. Landgraf, R. Snel, P. Tol, P. Ingmann, R.Voors, B. Kruizinga, R. Vink, H. Visser, P.F. Levelt, Remote Sens. Environ., **120**, 70–83 (2012)
32. N. Gorelick, M. Hancher, M. Dixon, S. Ilyushchenko, D. Thau, R. Moore, Remote Sens. Environ., **202**, 18–27 (2017)
33. D. Zanaga, R. Van De Kerchove, D. Daems, W.De Keersmaecker, C. Brockmann, G. Kirches, J. Wevers, O. Cartus, M. Santoro, S. Fritz, M. Lesiv, M. Herold, N.E. Tsendbazar, P. Xu, F. Ramoino, O. Arino, ESA WorldCover 10 m 2021 v200 (2022) doi: 10.5281/zenodo.7254221
34. D. Runfola, A. Anderson, H. Baier, M. Crittenden, E. Dowker, S. Fuhrig, S. Goodman, G. Grimsley, R. Layko, G. Melville, M. Mulder, R. Oberman, J. Panganiban, A. Peck, L. Seitz, S. Shea, H. Slevin, R. Youngerman, L. Hobbs, PLoS ONE, **15**, e0231866 (2020)
35. O. Nikitin, N. Stepanova, R. Kuzmin, E. Nasyrova, V. Latypova, E3S Web Conf., **498**, 02008 (2024)
36. O.V. Nikitin, E.I. Nasyrova, V.R. Nuriakhmetova, N.Yu. Stepanova, N.V. Danilova, V.Z. Latypova, IOP Conf. Ser.: Earth Environ. Sci., **107**, 012068 (2018)
37. O. Nikitin, E. Nasyrova, A. Kalinina, V. Latypova, 19th International Multidisciplinary Scientific Geoconference, SGEM 2019, **19**, 229–236 (2019)
38. B.R. Deemer, M.A. Holgerson, J. Geophys. Res. Biogeosci., **126**, e2019JG005600 (2021)
39. J.J. Beaulieu, T. DelSontro, J.A. Downing, Nat. Commun., **10**, 1375 (2019)
40. Y. Li, J.H. Shang, C. Zhang, W.L. Zhang, L.H. Niu, L.F. Wang, H.J. Zhang, Sci. Total Environ., **768**, 144582 (2021)
41. T.V. Turutina, A.V. Rakhuba, M.V. Shmakova, IOP Conf. Ser.: Earth Environ. Sci., **834**, 012001 (2021)
42. K.V. Selezneva, A.V. Selezneva, V.A. Seleznev, E3S Web Conf., **480**, 02022 (2024)
43. T. DelSontro, J.J. Beaulieu, J.A. Downing, Limnol. Oceanogr. Lett., **3**, 64–75 (2018)
44. P. Upadhyay, S.K. Prajapati, A. Kumar, Ecol. Indic., **154**, 110649 (2023)
45. E. Perez-Coronel, J.M. Beman, Nat. Commun., **13**, 6454 (2022)
46. A.M. Alowaifeer, Q. Wang, B. Bothner, R.J. Sibert, S.B. Joye, T.R. McDermott, Limnol. Oceanogr., **68**, 1762–1774 (2023)
47. S. Ma, M. Yang, X. Chen, F. Wang, Y. Xia, P. Xu, J. Ma, C. Luo, C. Zhou, T. Xu, Y. Zhu, J. Environ. Manag., **355**, 120481 (2024)
48. Y. Mao, T. Lin, H. Li, R. He, K. Ye, W. Yu, Q. He, Sci. Total Environ., **907**, 167864 (2024)